

Tensor Network Finite-Size Scaling for Two-Dimensional 3-state Clock Model

Debasmita Maiti¹, Sing-Hong Chan¹, Pochung Chen^{1,2,3}

¹ Department of Physics, National Tsing Hua University, Hsinchu 30013, Taiwan

² Physics Division, National Center for Theoretical Sciences, Taipei 10617, Taiwan

³ Frontier Center for Theory and Computation, National Tsing Hua University, Hsinchu 30013, Taiwan

E-mail: pcchen@phys.nthu.edu.tw

Abstract. We benchmark recently proposed tensor network based finite-size scaling analysis in Phys. Rev. B **107**, 205123 (2023) against two-dimensional classical 3-state clock model. Due to the higher complexity of the model, more complicated crossover behavior is observed. We advocate that the crossover behavior can be understood from the perspective of finite bond dimension inducing relevant perturbation. This leads to a general strategy to best estimate the critical properties for a given set of control parameters. For the critical temperature T_c , the relative error at the order of 10^{-7} can be reached with bond dimension $D = 70$. On the other hand, with bond dimension $D = 60$, the relative errors of the critical exponents ν, β, α are at the order of 10^{-2} . Increasing the bond dimension to $D = 90$, these relative errors can be reduced at least to the order of 10^{-3} . In all cases our results indicate that the errors can be systematically reduced by increasing the bond dimension and the stacking number.

Keywords: Finite-size scaling, Tensor network renormalization, 3-State clock model

Submitted to: *New J. Phys.*

1. Introduction

Tensor network methods have emerged as a powerful tool to study classical and quantum phase transitions [1]. For two-dimensional (2D) classical models, by representing the partition function as a tensor network and performing tensor renormalization, the nature of the phase transitions can be studied [2, 3, 4, 5, 6]. An advantage of the tensor network study of the classical models is that extremely large system size can be reached. This effectively reaches the thermodynamic limit, where the spontaneous symmetry breaking can occur. Consequently, the nature of the phase can be studied without using finite-size scaling analysis. Moreover, it is possible to identify fixed-point tensor from which critical properties can be extracted [7, 8, 9, 10, 11, 12, 13]. The core of these methods is the scheme to renormalize tensors. In recent year, various tensor

renormalization schemes have been proposed and studied. This includes Levin-Nave tensor renormalization group (LN-TRG) [14], higher-order tensor renormalization group (HOTRG) [15, 16], corner transfer matrix renormalization group (CTMRG) [17, 18], tensor network renormalization (TNR) [7] and loop-optimization of tensor network renormalization (loop-TNR) [19].

Due to the complexity of the 2D tensor contraction, it is necessary to introduce at least one control parameter D , called bond dimension, to make the calculation trackable. For some schemes, multiple bond dimensions are used. The finite bond dimension is related to the expressivity and entanglement entropy of the tensor network. As a result, the accuracy of the tensor contraction depends on the bond dimension. For extremely large-size calculations, the only length scale is induced by the bond dimension, and it is possible to perform scaling analysis in terms of the bond dimension. [20, 10, 5, 21]. Since the entanglement is finite due to the finite bond dimension, this is referred to as the finite-entanglement scaling regime [22, 20]. On the other hand, it is also possible to perform conventional finite-size scaling analysis, provided that the bond dimension is large enough so that the finite bond dimension effect can be neglected [23, 24, 25, 26, 21]. This is referred to as the finite-size scaling regime. In Ref. [25] some of us propose a scheme to perform tensor network based finite-size scaling analysis for the 2D Ising model. It is shown that critical temperature and critical exponents can be accurately estimated. More importantly, it is possible to systematically improve the results by increasing the bond dimension.

In this work, we generalize the idea in Ref. [25] to a general scheme to determine the critical temperature and critical exponents without a priori knowledge. Furthermore, we demonstrate that it is important to preserve the symmetry during tensor renormalization, especially for the estimation of critical exponent associated with the order parameter. Specifically, we benchmark against the 3-state clock model. It is well known that q -state clock [27] and Potts models [28] are two families of important classical statistical models, which exhibit many of fascinating features of critical phenomena. These models serve an important role to study critical phenomena in not only condensed matter physics, but also in high energy physics and bio physics [29, 28]. For $q = 2$ both models are equivalent to the Ising model, while for $q = 3$ they are the same after a rescaling of the coupling constant [28]. They have been extensively investigated both analytically and numerically [30, 29, 31, 32, 33, 34, 35]. Moreover, in recent years tensor network techniques have been used to study various aspects of the q -state clock and Potts models [3, 30, 36, 4, 5, 37]. Here we investigate 3-state ferromagnetic clock model by using HOTRG method employing finite-size scaling. While a more complex crossover behavior is observed, it is shown later in this work that by using the general scheme described below, accurate results can be obtained.

In the following we briefly describe our main strategy. In general we consider some physical quantity Q . It is expected that Q satisfies a finite-size scaling of the form

$$Q(L_y) = Q(\infty) + a_0 L_y^{-\omega_0} + a_1 L_y^{-\omega_1} + \dots, \quad (1)$$

where L_y is the system size, $Q(\infty)$ is its thermodynamical value, a_i s are non-universal constants, and $\omega_0 < \omega_1 < \dots$ represent the leading and higher order corrections to the scaling. Typically one estimates $Q(\infty)$ either by fitting $Q(L_y)$ to Eq. 1 or by using $Q(L_y)$ at the largest L_y available. If the quantity $Q(L_y)$ is evaluated exactly, one expects that Q approaches $Q(\infty)$ monotonically. On the other hand, for tensor renormalization based calculations, typically one finds that initially Q flows toward $Q(\infty)$ monotonically but it start to flow away from $Q(\infty)$ after certain length scale. From the real-space renormalization group perspective, we attribute this to the finite bond dimension induced relevant perturbation [21]. In the beginning the relevant perturbation is weak and the system flows toward the fixed point as one increases the system size. However, during the renormalization the relevant perturbation also becomes stronger. Eventually the system starts to flow away from the fixed point.

Our main strategy is to identify the perihelion of the renormalization trajectory, i.e., the system size at which the system is closest to the fixed point. We find it natural to consider $\frac{dQ}{d \ln L_y}$. For exact calculation without relevant perturbation one expects that the magnitude of $\frac{dQ}{d \ln L_y}$ decreases monotonically to zero as system size increases. In the presence of relevant perturbation, however, $\frac{dQ}{d \ln L_y}$ decreases monotonically to a minimal value at certain length scale L_y^* , then it starts to increase. We argue that L_y^* corresponds to the perihelion of the renormalization trajectory of Q and we use $Q(L_y^*)$ as the best estimation of Q .

In practice we first determine the critical temperature T_c by using the crossing point of the dimensionless ξ/L_y , where ξ is the correlation length. It is known that the crossing point of dimensionless quantity converges faster to T_c due to the cancellation of the leading order correction. Our results indicate that T_c can be determined with extremely high accuracy. On the other hand, there are two types of scaling which can be used to estimate the critical exponents. First type of method relies on the temperature derivative of some physical quantity, evaluated at a sequence of temperatures. The requirement is that the temperature sequence shall converge to the critical temperature. A common sequence to use is the sequence of finite-size crossing point. The advantage is that a priori knowledge of exact T_c is not required. Second type of method relies on evaluating some physical quantity at T_c . Since extremely high accuracy can be reached for T_c , we propose that for both types of methods one can perform the scaling analysis at the above mentioned best estimation of T_c . However, to better understand the intrinsic error and the error due to non-exact T_c , in this work we first estimate the critical exponents by sitting at exact T_c . But we also perform the same scaling analysis with non-exact T_c . Our results show that the error due to non-exact T_c is much smaller than other intrinsic error.

Finally we would also like to comment on the effect of corner double-line (CDL) tensors before presenting our results. It is known that CDL tensors contain only ultra-short-range correlator [11]. However, some tensor renormalization methods such as LN-TRG and HOTRG cannot filter out CDL tensors [11, 10]. Conceptually this presents

a problem if one is seeking a fixed point tensor. The existence of CDL tensors means that a phase is described by a class of equivalent fixed-point tensors instead of by a unique fixed-point tensor. However, since our approach is based on the finite-size scaling behavior of physical quantities this is not a problem [38]. In practice the existence of CDL tensors indicates that part of the computational resources is used to represent and process CDL tensors. For tensor renormalization methods which can filter out the CDL tensors, it is likely that the same accuracy can be reached with smaller bond dimension. However, these methods are also more complex computationally. Hence, it remains to be investigated which tensor renormalization method can lead to best results within the same limit of computational resource.

The rest of the manuscript is organized as follows: In Sec. 2 we briefly describe the model and summarize the exact results for critical properties. The information of the construction and renormalization of the tensor is also given. In Sec. 3 we present our numerical results for the critical temperature T_c and critical exponents ν , β , α and crossover length scale. We then conclude and provide some further discussion in Sec. 4.

2. Model and method

We consider 2D classical ferromagnetic 3-state clock model on a square lattice with the Hamiltonian

$$H_{\text{clock}}[\{\theta\}] = -J \sum_{\langle i,j \rangle} \cos(\theta_i - \theta_j), \quad (2)$$

where $J > 0$, $\theta_i \in \{0, \frac{2\pi}{3}, \frac{4\pi}{3}\}$, and $\langle i, j \rangle$ denotes nearest neighbors. The model exhibits a continuous phase transition from the high-temperature disordered phase to the low-temperature ordered phase. The exact critical temperature and critical exponents are known, with $k_B T_c = \frac{3}{2} \frac{1}{\ln(1+\sqrt{3})} \approx 1.49246$, $\nu = \frac{5}{6} = 0.8\bar{3}$, $\beta = \frac{1}{9} = 0.\bar{1}$. and $\alpha = \frac{1}{3} = 0.\bar{3}$ [28]. For the convenience of the finite-size scaling analysis, it is also convenient to quote following values: $\frac{1}{\nu} = \frac{6}{5} = 1.2$, $\frac{\beta}{\nu} = \frac{2}{15} = 0.1\bar{3}$, $\frac{\alpha}{\nu} = \frac{2}{5} = 0.4$, and $\frac{1-\beta}{\nu} = \frac{16}{15} = 1.0\bar{6}$.

In this work, we apply the tensor network based finite-size scaling analysis proposed in Ref. [25] to determine the critical temperature and the critical exponents. We start from the tensor network representation of the partition function

$$Z = \sum_{\{\theta\}} e^{-\beta H[\{\theta\}]} = \text{tTr} \prod_{\text{sites}} \mathbf{T}_{ijkl}, \quad (3)$$

where β is the inverse temperature and tTr is the tensor trace. \mathbf{T}_{ijkl} , where $i, j, k, l \in \{0, 1, 2\}$, is the local tensor. For the 3-state clock model, the local tensor reads [36]

$$\mathbf{T}_{ijkl} = \frac{\sqrt{\lambda_i \lambda_j \lambda_k \lambda_l}}{3} \delta_{\text{mod}(i+j-k-l, 3)}, \quad (4)$$

where

$$\lambda_m = \sum_{\theta_i} \cos(m\theta_i) e^{\beta J \cos(\theta_i)}. \quad (5)$$

Following Ref [25], we first perform exact contraction of 2×2 or 3×3 sites of \mathbf{T} tensors to construct a $\mathbf{T}^{(d,0)}$ tensor, where $d = 2, 3$ is the initial block size. Then we use HOTRG to coarse-grain the tensor iteratively. After N iterations, one obtains the renormalized tensor $\mathbf{T}^{(d,N)}$ which represents approximately $L \times L$ sites of \mathbf{T} tensors where $L = d * 2^N$. By stacking n copies of the $\mathbf{T}^{(d,N)}$ tensors vertically and tracing out the vertical bonds, one obtains the transfer matrix \mathcal{T}_{L,L_y} . It represents a column-to-column transfer matrix with $L_y = nL$ sites, raised to the power of L . In the following we denote the eigenvalue and the eigenvector of \mathcal{T}_{L,L_y} as $\lambda_i(L, L_y)$ and $|\lambda_i(L, L_y)\rangle$ respectively, where λ_i is sorted in descending order. By defining $E_i(L_y) = -\ln(\lambda_i(L, L_y))/L$, the correlation length associated with an infinite strip with width L_y can be evaluated as $\xi = \frac{1}{E_1 - E_0}$.

The 3-state clock model possesses a \mathbb{Z}_3 symmetry. Due to the symmetry, the magnetization is exactly zero for any finite L_y . At critical temperature, however, it is possible to define a pseudo spontaneous magnetization m [39]. First define an impurity tensor with following elements

$$\mathbf{T}_{ijkl}^{z\pm} = \frac{\sqrt{\lambda_i \lambda_j \lambda_k \lambda_l}}{3} \delta_{\text{mod}(i+j-k-l \pm 1, 3)}, \quad (6)$$

and renormalize it alongside \mathbf{T} to obtain the renormalized $\mathbf{T}_z^{(d,N)}$. Next, one constructs a $\mathcal{T}_{L,L_y}^{z\pm}$ matrix by stacking $n - 1$ copies of the $\mathbf{T}^{(d,N)}$ tensors and one $\mathbf{T}_{z\pm}^{(d,N)}$ vertically and tracing out the vertical bonds. The pseudo spontaneous magnetization m is then defined as the smallest eigenvalue of the matrix

$$\begin{pmatrix} \langle \lambda_0 | \mathcal{T}_{L,L_y}^z | \lambda_0 \rangle & \langle \lambda_0 | \mathcal{T}_{L,L_y}^z | \lambda_1 \rangle & \langle \lambda_0 | \mathcal{T}_{L,L_y}^z | \lambda_2 \rangle \\ \langle \lambda_1 | \mathcal{T}_{L,L_y}^z | \lambda_0 \rangle & \langle \lambda_1 | \mathcal{T}_{L,L_y}^z | \lambda_1 \rangle & \langle \lambda_1 | \mathcal{T}_{L,L_y}^z | \lambda_2 \rangle \\ \langle \lambda_2 | \mathcal{T}_{L,L_y}^z | \lambda_0 \rangle & \langle \lambda_2 | \mathcal{T}_{L,L_y}^z | \lambda_1 \rangle & \langle \lambda_2 | \mathcal{T}_{L,L_y}^z | \lambda_2 \rangle \end{pmatrix}, \quad (7)$$

where $\mathcal{T}^z \equiv \mathcal{T}^{z+} + \mathcal{T}^{z-}$.

Due to the \mathbb{Z}_3 symmetry, the transfer matrix \mathcal{T}_{L,L_y} is block diagonal and can be decomposed into three blocks with \mathbb{Z}_3 charge $Q = 0, 1, 2$ respectively. It turns out that $|\lambda_0\rangle, |\lambda_1\rangle, |\lambda_2\rangle$ have $Q = 0, 1, 2$ respectively and E_1 and E_2 are degenerate. Since \mathcal{T}_{L,L_y}^z changes \mathbb{Z}_3 charge by ± 1 , the diagonal elements $\langle \lambda_i | \mathcal{T}_{L,L_y}^z | \lambda_i \rangle$ should be zero, if symmetric eigenvectors are used. However, if symmetry is not enforced during the tensor renormalization, numerical inaccuracy and truncation may lead to \mathbb{Z}_3 symmetry breaking and diagonal elements become non-zero. Based on these observations we use the sum $\sum_{q=0,1,2} \langle \lambda_q | \mathcal{T}_{L,L_y}^z | \lambda_q \rangle$ as a measure to gauge the effect of these unintentional symmetry breaking. As it is shown later that this quantity may suddenly become larger after some tensor renormalization and make the calculation of the magnetization unstable.

3. Numerical Results and Finite-Size Scaling Analysis

3.1. Critical temperature T_c

Following conventional finite-size scaling analysis, we first use the crossing point of the dimensionless ξ/L_y to estimate the critical temperature T_c . In Figure 1, ξ/L_y is plotted

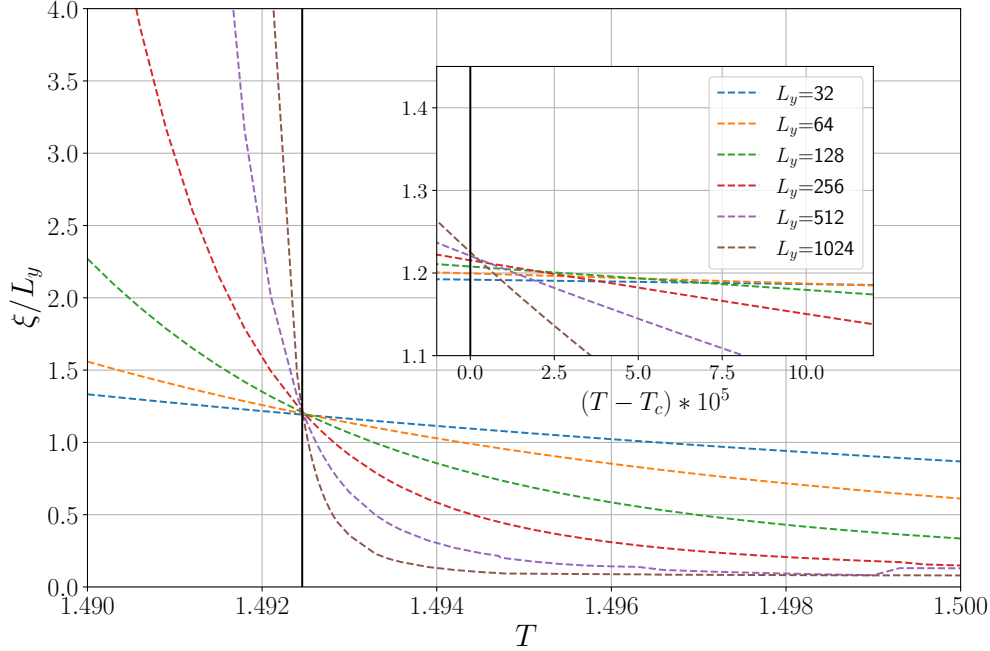


Figure 1. ξ/L_y as a function of T with various L_y , obtained with $D = 70$ and $n = 3$. Inset: Zoomed plot near T_c .

as a function of the temperature T for various L_y , where $D = 70$ and $n = 3$ are used. As expected, curves from different sizes cross near T_c which is indicated by the vertical black line. In the inset, we zoom in near T_c and the drifting of the crossing point is clearly observed. It is common to define the crossing point of $\xi(L_y)/L_y$ and $\xi(2L_y)/(2L_y)$ as $T^*(L_y)$, which represents the finite-size estimation of T_c and it approaches T_c as $L_y \rightarrow \infty$. Based on our general strategy, we plot the relative error $\frac{T^*}{T_c} - 1$ and $\left| \frac{dT^*}{d\ln(L_y)} \right|$ respectively as a function of $\ln(L_y)$ in Figure 2(a) and (b). Here only results from $D = 50, 60, 70$, and $n = 3$ are plotted for clarity. It should be noted that the labels for y-axis in Figure 2(a) is at the order of 10^{-5} . We observe that T^* flows toward T_c for smaller L_y , but it starts to flow away for larger L_y . Similarly, we find that $\left| \frac{dT^*}{d\ln(L_y)} \right|$ decreases monotonically toward zero for smaller L_y , but for larger L_y it shows non-monotonic behavior. This can be attributed to the crossover between finite-size scaling regime and finite-entanglement scaling regime [25]. As discussed in the introduction, we define L_y^* to be the size at which $\left| \frac{dT^*}{d\ln(L_y)} \right|$ attains its first local minimum as L_y increases and use $T^*(L_y^*)$ as the best estimation of T_c for a fixed D and n . We emphasize that the procedure does not require a priori knowledge of exact T_c . The dashed line in Figure 2(a), which corresponds to the exact value, is plotted only as a reference. Moreover, we find that $T^*(L_y)$ is quite flat near L_y^* and it would be desirable to have more data near L_y^* to obtain a better estimation. However, one cannot evaluate T^* at all possible L_y due to the nature of

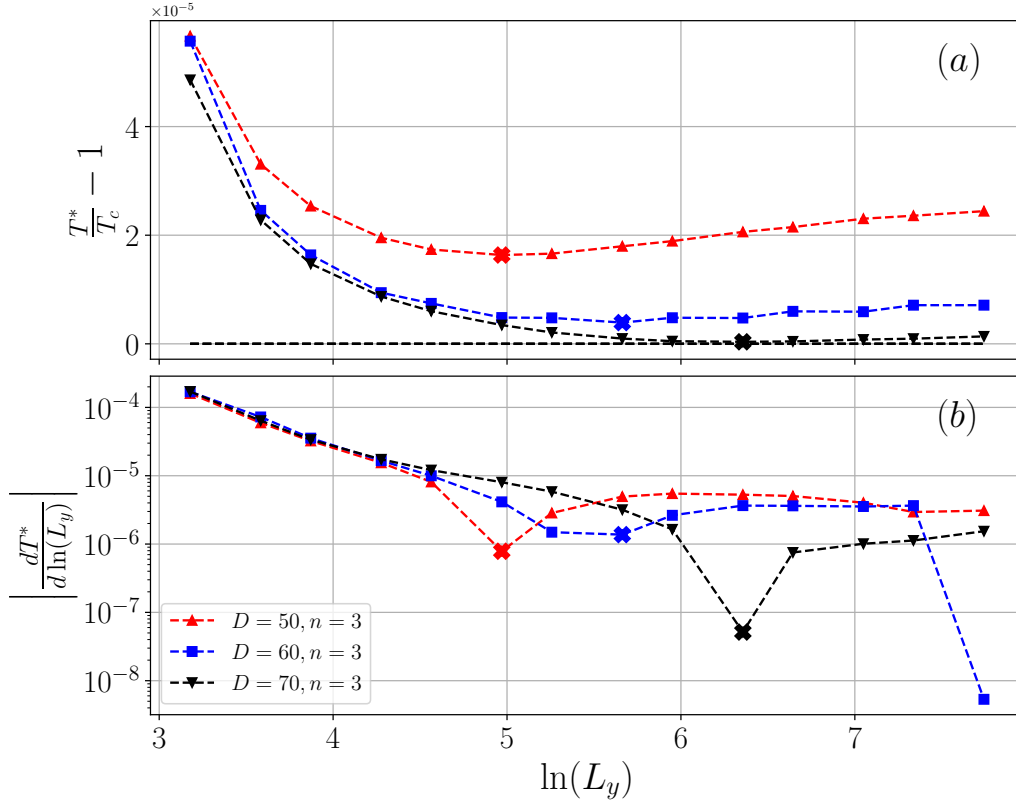


Figure 2. (a) $\frac{T^*}{T_c} - 1$ as a function of $\ln(L_y)$. Horizontal dashed line corresponds to the exact value. Dashed lines connecting symbols are guides for the eye. (b) $\left| \frac{dT^*}{d \ln(L_y)} \right|$ as a function of $\ln(L_y)$. The crosses indicate the L_y^* where $\left| \frac{dT^*}{d \ln(L_y)} \right|$ attains its first local minimum.

HOTRG. Consequently the L_y^* obtained here only represents a rough estimation of the crossover length scale.

In Table 1, we summarize our results of the L_y^* and the relative error $\frac{T^*}{T_c} - 1$. We find that the error can be systematically improved by increasing D or n . With $D = 50$ and $n = 1$, the relative error is already at the order of 10^{-5} which is quite small. With $D = 70$ and $n = 3$, the relative error can be further reduced to the order of 10^{-7} . Our results indicate that T_c can be estimated with extremely high accuracy. Finally we note that results from \mathbb{Z}_3 symmetric HOTRG are presented here. We have also performed the calculations in which the \mathbb{Z}_3 symmetry is not explicitly preserved. We find that the identification of L_y^* remains the same and relative error is of the same order.

Table 1. Summary of the relative error $\epsilon_T \equiv \frac{T^*}{T_c} - 1$.

D	L_y^*	ϵ_T	L_y^*	ϵ_T	L_y^*	ϵ_T
50	256	$+1.97 \times 10^{-5}$	192	$+1.83 \times 10^{-5}$	144	$+1.63 \times 10^{-5}$
60	512	$+6.73 \times 10^{-6}$	256	$+4.72 \times 10^{-6}$	288	$+3.91 \times 10^{-6}$
70	768	$+6.51 \times 10^{-7}$	512	-2.64×10^{-9}	576	$+3.70 \times 10^{-7}$

3.2. Critical exponent ν

To estimate the critical exponent ν , we first define the finite-size estimation of $\frac{1}{\nu}$ as

$$\left(\frac{1}{\nu}\right)^* \equiv \frac{\ln S_{\xi/L_y}(2L_y) - \ln S_{\xi/L_y}(L_y)}{\ln(2)}, \quad (8)$$

where $S_{\xi/L_y} \equiv \left. \frac{d}{dT} \left(\frac{\xi}{L_y} \right) \right|_{T_c}$ is the slope of $\frac{\xi}{L_y}$ at T_c [25]. Based on the finite-size scaling theory, it is expected that $\left(\frac{1}{\nu}\right)^*$ should approach the exact value $\frac{1}{\nu} = \frac{6}{5}$ in the thermodynamic limit. Following again the general strategy, in Figure 3(a) we plot the relative error $\left(\frac{1}{\nu}\right)^* / \left(\frac{1}{\nu}\right) - 1$ as a function of $\ln(L_y)$, while in Figure 3(b) we plot $\left| \frac{d(1/\nu)^*}{d \ln(L_y)} \right|$. The results follow the general trend as described in the introduction and are similar to the results of T^* . To identify the perihelion of the renormalization trajectory of $\left(\frac{1}{\nu}\right)^*$, we locate the size L_y^* at which $\left| \frac{d(1/\nu)^*}{d \ln(L_y)} \right|$ attains its first local minimum as L_y increases. Then $\left(\frac{1}{\nu}\right)^*$ at L_y^* is used as the best estimation of $\frac{1}{\nu}$ for a fixed set of parameters. In Table 2 we summarize our results for the relative error. With $D = 60$ and $n = 1$, the relative error is about 10^{-3} which is small. By using $D = 90$ and $n = 3$, it can be further reduced to the order of 10^{-4} . An interesting observation is that the L_y^* identified here is very different from the one identified via T^* . As one sees from the results of other critical exponents, the value and the trend of L_y^* are different for different physical quantity. Finally we note that the results from \mathbb{Z}_3 symmetric HOTRG are presented here and the results from non-symmetry-preserving HOTRG are similar.

Some additional comments are now in order. In the estimation of $1/\nu$ above, we evaluate the slope in Eq. 8 at exact T_c . This is because we would like to investigate the intrinsic error due to the tensor renormalization. In general the exact T_c is not known. In this case, we advocate that the best strategy is to estimate the critical exponents based on the quantities evaluated at the best estimated T_c , i.e., $T^*(L_y^*)$. This is based on the observation that T_c can be estimated with extremely high accuracy and the error of the critical exponent is much larger than the error of critical temperature. To further support this, we have performed the same analysis but with data evaluated at temperature shifted away from T_c by an order of 10^{-5} to account for the error in the estimated value of T_c . First, we find that the same L_y^* is identified. Furthermore, while in general the relative error increases, it typically remains within the same order of magnitude. These results indicate that the error due to using non-exact T_c is much smaller than the intrinsic error, in support of our claim.

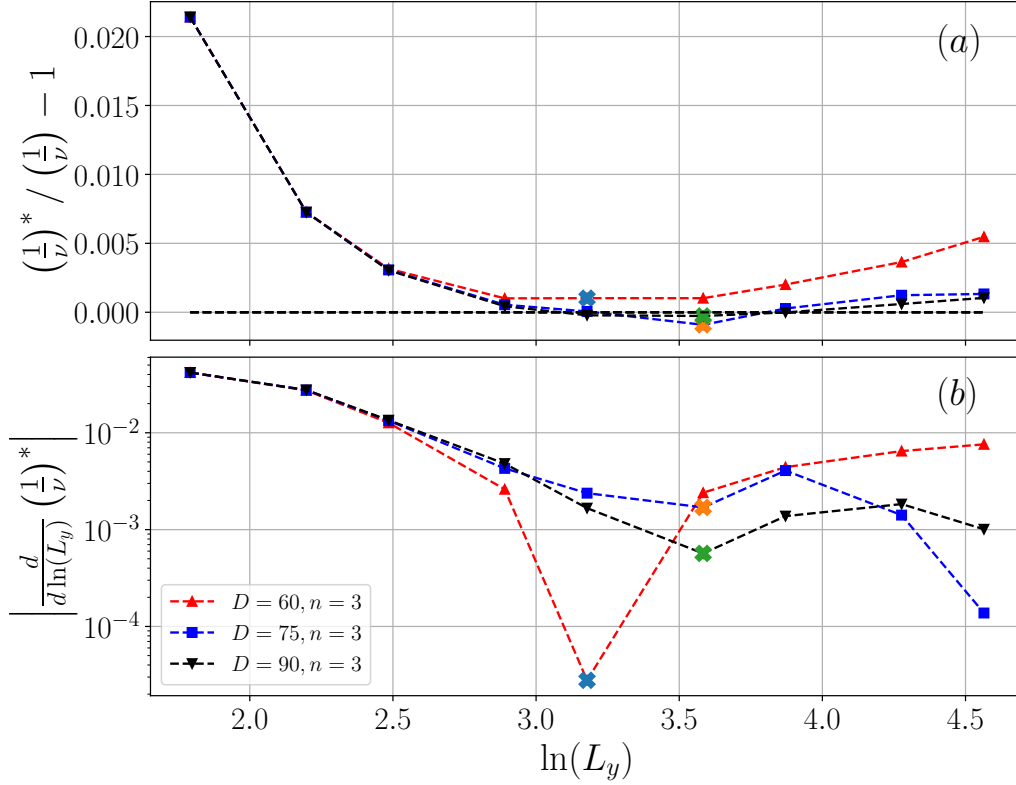


Figure 3. (a) $(\frac{1}{\nu})^* / (\frac{1}{\nu}) - 1$ as a function of $\ln(L_y)$. Horizontal dashed line corresponds to the exact value. Dashed lines connecting symbols are guides for the eye. (b) $\left| \frac{d}{d \ln(L_y)} (\frac{1}{\nu})^* \right|$ as a function of $\ln(L_y)$. The crosses indicate the L_y^* where $\left| \frac{d}{d \ln(L_y)} (\frac{1}{\nu})^* \right|$ attains its first local minimum.

Table 2. Summary of the relative error $\epsilon_\nu \equiv (\frac{1}{\nu})^* / (\frac{1}{\nu}) - 1$.

D	L_y^*	ϵ_ν	L_y^*	ϵ_ν	L_y^*	ϵ_ν
60	16	$+7.86 \times 10^{-3}$	24	$+1.99 \times 10^{-3}$	24	$+1.02 \times 10^{-3}$
75	16	$+3.96 \times 10^{-3}$	24	-4.44×10^{-4}	36	-9.12×10^{-4}
90	16	$+4.69 \times 10^{-3}$	24	$+3.07 \times 10^{-4}$	36	-2.70×10^{-4}

3.3. Critical exponent β

In this work we use two approaches to estimate the critical exponent β . First approach uses the slope of the pseudo spontaneous magnetization m at T_c to estimate $\frac{1-\beta}{\nu}$. Similar to the finite-size estimation of $\frac{1}{\nu}$, we define the finite-size estimation of $\frac{1-\beta}{\nu}$ as

$$\left(\frac{1-\beta}{\nu} \right)^* \equiv \frac{\ln S_m(2L_y) - \ln S_m(L_y)}{\ln(2)}, \quad (9)$$

where $S_m \equiv \left. \frac{dm}{dT} \right|_{T_c}$ is the slope of the m at T_c . Second approach uses the finite-size

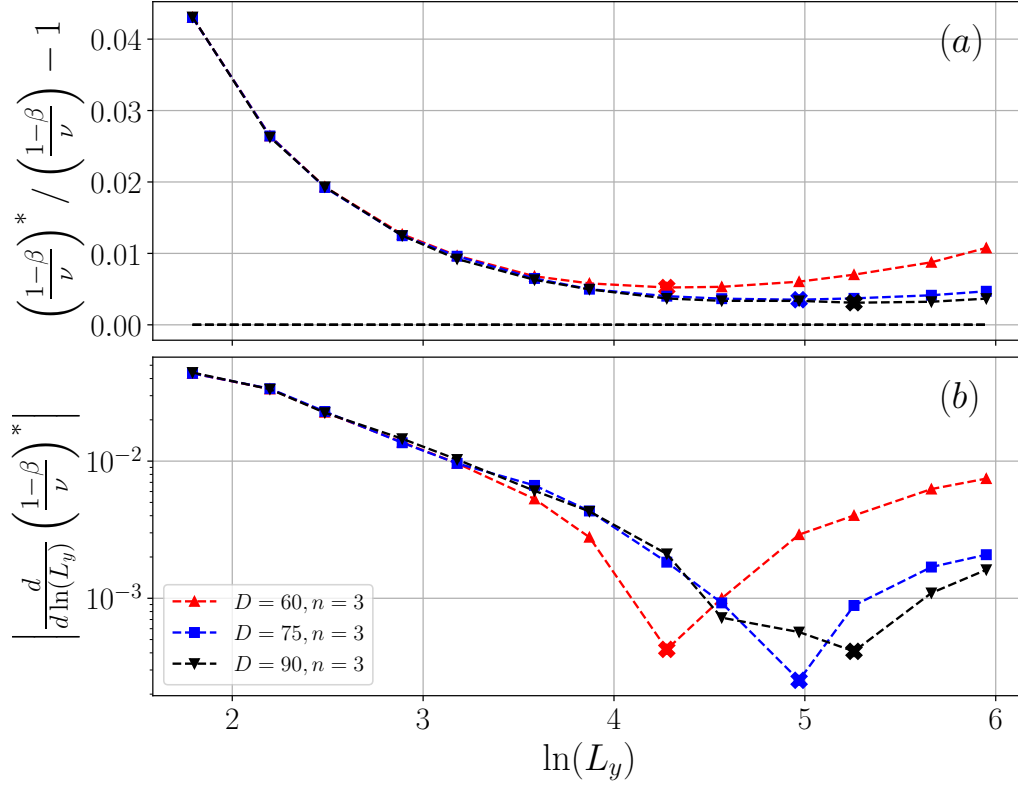


Figure 4. (a) $\left(\frac{1-\beta}{\nu}\right)^* / \left(\frac{1-\beta}{\nu}\right) - 1$ as a function of $\ln(L_y)$. Horizontal dashed line corresponds to the exact value. Dashed lines connecting symbols are guides for the eye. (b) $\left|\frac{d}{d\ln(L_y)} \left(\frac{1-\beta}{\nu}\right)^*\right|$ as a function of $\ln(L_y)$. The crosses indicate the L_y^* where $\left|\frac{d}{d\ln(L_y)} \left(\frac{1-\beta}{\nu}\right)^*\right|$ attains its first local minimum.

scaling behavior of m at T_c to estimate β . Since one expects $m(T_c, L_y) \propto L_y^{-\beta/\nu}$, we define the finite-size estimation of $\frac{\beta}{\nu}$ as

$$\left(\frac{\beta}{\nu}\right)^* \equiv -\frac{d\ln(m(T_c, L_y))}{d\ln(L_y)}, \quad (10)$$

and evaluate it numerically. In the thermodynamic limit, it is expected that $\left(\frac{1-\beta}{\nu}\right)^* \rightarrow \frac{1-\beta}{\nu} = \frac{16}{15}$ and $\left(\frac{\beta}{\nu}\right)^* \rightarrow \frac{\beta}{\nu} = \frac{2}{15}$. In Figure 4(a) and 5(a) we plot respectively the relative error $\left(\frac{1-\beta}{\nu}\right)^* / \left(\frac{1-\beta}{\nu}\right) - 1$ and $\left(\frac{\beta}{\nu}\right)^* / \left(\frac{\beta}{\nu}\right) - 1$ as a function of $\ln(L_y)$, where the dashed line corresponds to the exact value. To identify L_y^* , we plot $\left|\frac{d}{d\ln(L_y)} \left(\frac{1-\beta}{\nu}\right)^*\right|$ in Figure 4(b) while $\left|\frac{d(\beta/\nu)^*}{d\ln(L_y)}\right|$ is plotted in Figure 5(b). Again we find it follows the general trend as described in the introduction and we assign L_y^* to be the size at which it attains first local minimum. We summarize the results in terms of relative error in Table 3 and Table 4.

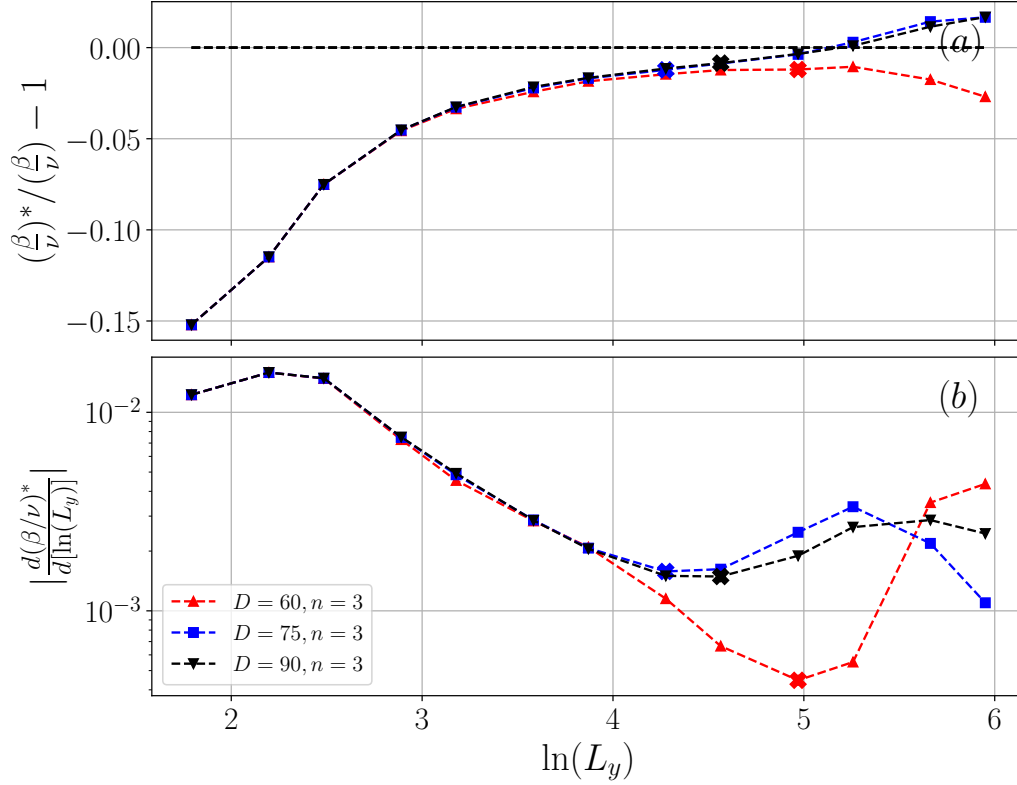


Figure 5. (a) $(\frac{\beta}{\nu})^* / (\frac{\beta}{\nu}) - 1$ as a function of $\ln(L_y)$. Horizontal dashed line corresponds to the exact value. Dashed lines connecting symbols are guides for the eye. (b) $|\frac{d(\beta/\nu)^*}{d \ln(L_y)}|$ as a function of $\ln(L_y)$. The crosses indicate the L_y^* where $|\frac{d(\beta/\nu)^*}{d \ln(L_y)}|$ attains its first local minimum.

Table 3. Summary of the relative error $\epsilon_{(1-\beta)} \equiv (\frac{1-\beta}{\nu})^* / (\frac{1-\beta}{\nu}) - 1$.

D	L_y^*	$\epsilon_{(1-\beta)}$	L_y^*	$\epsilon_{(1-\beta)}$	L_y^*	$\epsilon_{(1-\beta)}$
60	32	$+1.52 \times 10^{-2}$	64	$+7.14 \times 10^{-3}$	72	$+5.22 \times 10^{-3}$
75	48	$+1.09 \times 10^{-2}$	96	$+5.12 \times 10^{-3}$	144	$+3.51 \times 10^{-3}$
90	48	$+7.77 \times 10^{-3}$	128	$+4.56 \times 10^{-3}$	192	$+3.10 \times 10^{-3}$

Table 4. Summary of the relative error $\epsilon_\beta \equiv (\frac{\beta}{\nu})^* / (\frac{\beta}{\nu}) - 1$.

D	L_y^*	ϵ_β	L_y^*	ϵ_β	L_y^*	ϵ_β
60	64	-3.28×10^{-2}	192	-1.16×10^{-2}	144	-1.20×10^{-2}
75	64	-2.74×10^{-2}	64	-1.50×10^{-2}	72	-1.22×10^{-2}
90	64	-2.41×10^{-2}	96	-9.97×10^{-3}	96	-8.51×10^{-3}

The results show that first approach has slightly better accuracy. The error of second approach is about two to three times larger. With $D = 60$, $n = 1$, the relative error is at the order of 10^{-2} . Pushing to $D = 90$, $n = 3$, the relative error is reduced to 10^{-3} , and the overall improvement is similar for both methods. We note that for both approaches results from HOTRG which explicitly preserves the \mathbb{Z}_3 symmetry are plotted here. On the other hand, we find that if the \mathbb{Z}_3 symmetry is not explicitly preserved in the HOTRG, the estimation of $(\frac{1-\beta}{\nu})^*$ becomes unstable for larger D while the estimation of $(\beta/\nu)^*$ remains stable. We attribute this instability to the accidental symmetry breaking. As mentioned in Sec. 2, one can use $\sum_q \langle \lambda_q | \mathcal{T}_{L, L_y}^z | \lambda_q \rangle$ to gauge the accidental symmetry breaking. In Figure 6 we plot this quantity at T_c as a function of $\ln(L_y)$ on a semilog plot using HOTRG which does not explicitly preserves the \mathbb{Z}_3 symmetry. We observe a smooth linear dependence for $D = 60$, but for $D = 75, 90$ there is a sudden jump of several order of magnitude at some length scale. The reason why this happens at larger D and L_y can be understood intuitively. As D and L_y increase the singular values in the tail also become smaller. This makes it easier to accidentally mix sectors with different quantum numbers during HOTRG, resulting the accidental symmetry breaking. Once accidental symmetry breaking occurs, the quantity shown in Figure 6 exhibits a sudden jump. However, exactly when such an accidental symmetry breaking occurs depends sensitively on various parameters. Consequently, the numerical derivative $\frac{dm}{dT}|_{T_c}$ and hence the estimation of $(\frac{1-\beta}{\nu})^*$ becomes numerically unstable at larger D and L_y . This observation shows that it is essential to explicitly keep the symmetry when estimating the exponent related to the order parameter.

3.4. Critical exponent α

To estimate critical exponent α , we start with $\mathbf{T}_{\langle i, j \rangle} \equiv \mathbf{T}_i^{z+} \mathbf{T}_j^{z-} + \mathbf{T}_i^{z-} \mathbf{T}_j^{z+}$ where i, j are nearest neighbours and renormalize it alongside \mathbf{T} . It is then straightforward to evaluate the energy per bond from the renormalized $\mathbf{T}^{(d, N)}$ and $\mathbf{T}_{\langle i, j \rangle}^{(d, N)}$. Next we perform numerical derivative to obtain the specific heat per site c_v , and the finite-size estimation of $(\frac{\alpha}{\nu})$ which is defined as

$$\left(\frac{\alpha}{\nu}\right)^* \equiv \frac{d \ln(c_v(T_c, L_y))}{d \ln(L_y)}. \quad (11)$$

In Figure 7(a) we plot the relative error $(\frac{\alpha}{\nu})^* / (\frac{\alpha}{\nu}) - 1$ as a function of $\ln(L_y)$, where the black dashed line corresponds to the exact value. We observe that $(\frac{\alpha}{\nu})^*$ shows a much stronger finite-size and larger system size is needed to reach similar relative error. Next we plot $\left| \frac{d}{d \ln(L_y)} \left(\frac{\alpha}{\nu}\right)^* \right|$ in Figure 7(b) and we use the same strategy to identify the length scale L_y^* and to estimate the exponent α . In Table. 5 we summarize our findings.

We note that results from \mathbb{Z}_3 symmetric calculations are presented here and calculations without enforcing \mathbb{Z}_3 symmetry becomes unstable to determine the exponent for larger L and D . This is because it is necessary to take two numerical steps to obtain $(\frac{\alpha}{\nu})^*$ and another one to obtain $\left| \frac{d}{d \ln(L_y)} \left(\frac{\alpha}{\nu}\right)^* \right|$, they become numerically less stable at larger L_y . Furthermore, while qualitatively the accuracy increases when

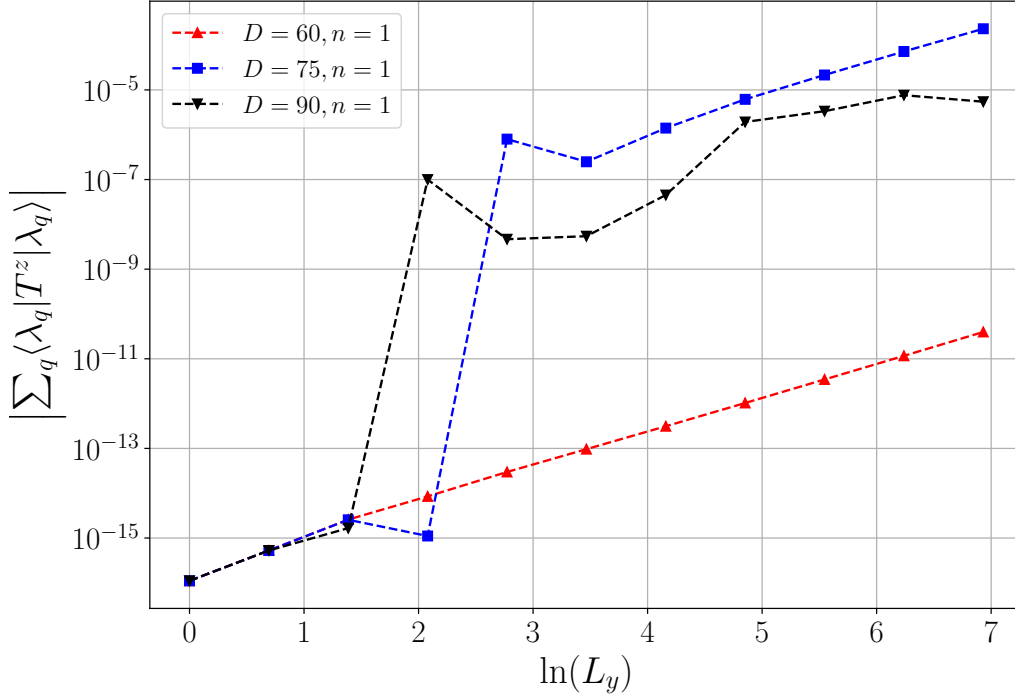


Figure 6. $\sum_q \langle \lambda_q | \mathcal{T}_{L, L_y}^z | \lambda_q \rangle$ as a function of $\ln(L_y)$. Dashed lines connecting symbols are guides for the eye.

Table 5. Summary of relative error $\epsilon_\alpha \equiv \left(\frac{\alpha}{\nu}\right)^* / \left(\frac{\alpha}{\nu}\right) - 1$.

D	L_y^*	ϵ_α	L_y^*	ϵ_α	L_y^*	ϵ_α
60	1024	2.39×10^{-2}	1024	1.31×10^{-2}	1152	6.04×10^{-4}
75	512	5.09×10^{-2}	1024	1.55×10^{-2}	1536	4.53×10^{-4}
90	1536	1.88×10^{-2}	1536	7.31×10^{-3}	1152	1.54×10^{-2}

D or n are increased, it becomes tricky to identify L_y^* . Consequently, best estimated exponents are not monotonic as one increases D or n . However, the accuracy is at least at the order of 10^{-2} and can be reduced to 10^{-4} .

3.5. Crossover length scale

Finally we would like to investigate if there exists a bond-dimension induced crossover length scale $\tilde{L}(D)$, which scales as D^κ and if the exponent κ agrees with the conventional expectation based on the conformal field theory [20, 10, 40, 2, 5]. From finite-size scaling theory one expects that for large enough L_y one has

$$\frac{E_i(L_y)}{L_y} = \beta_c f_c^\infty + a_i \frac{1}{L_y^2} + \dots, \quad (12)$$

where a_i s are non-universal. With a finite bond-dimension D , however, the length scale

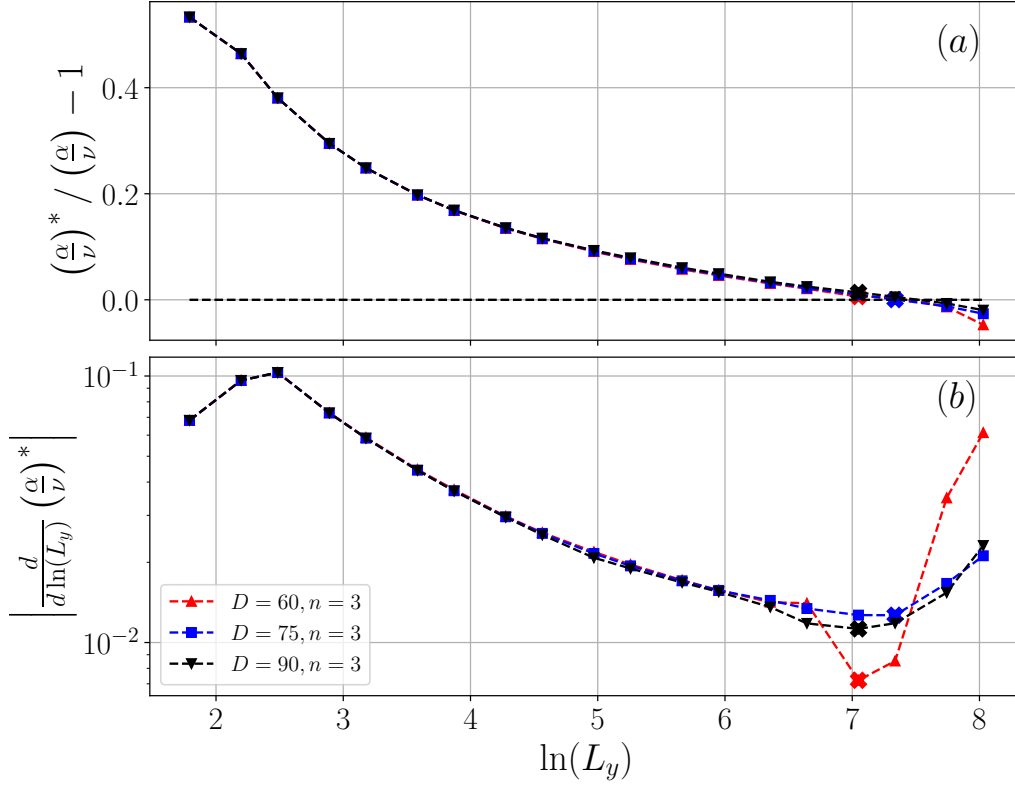


Figure 7. (a) $\left(\frac{\alpha}{\nu}\right)^* / \left(\frac{\alpha}{\nu}\right) - 1$ as a function of $\ln(L_y)$. Horizontal dashed line corresponds to the exact value. Dashed lines connecting symbols are guides for the eye. (b) $\left| \frac{d}{d \ln(L_y)} \left(\frac{\alpha}{\nu}\right)^* \right|$ as a function of $\ln(L_y)$. The crosses indicate the L_y^* where it attains its first local minimum.

L_y in the right hand side should be replaced by $\tilde{L}(D)$ and the equation becomes

$$\lim_{L_y \rightarrow \infty} \frac{E_i(L_y, D)}{L_y} = \beta_c f_c^\infty + \tilde{a}_i \frac{1}{D^{2\kappa}} + \dots \quad (13)$$

For a fixed D we iterate the HOTRG process until $E_i(L_y, D)/L_y$ converges and the results are plotted as a function of D in Figure 8. We then fit the results to Eq. 13, where $\beta_c f_c^\infty$, \tilde{a}_i , and 2κ are fitting parameters. We find $\beta_c f_c^\infty \approx -1.4001518(7)$ and $2\kappa \approx -3.00(4)$ consistently for $i = 0, 1, 2$. On the other hand, the expectation based on the conformal field theory is

$$\kappa_{\text{CFT}} = \frac{6}{c \left(\sqrt{\frac{12}{c}} + 1 \right)}, \quad (14)$$

where c is the central charge associated with the critical point. With $c = 4/5$ for the 3-state clock model, one has $2\kappa_{\text{CFT}} \approx 3.0782$, which is close to our fitted value. We have also tried to directly identify $\tilde{L}(D)$ similar to Ref. [25]. We find that due to the finite accuracy of fitted $\beta_c f_c^\infty$, one cannot reliably estimate $\tilde{L}(D)$ especially for larger D .

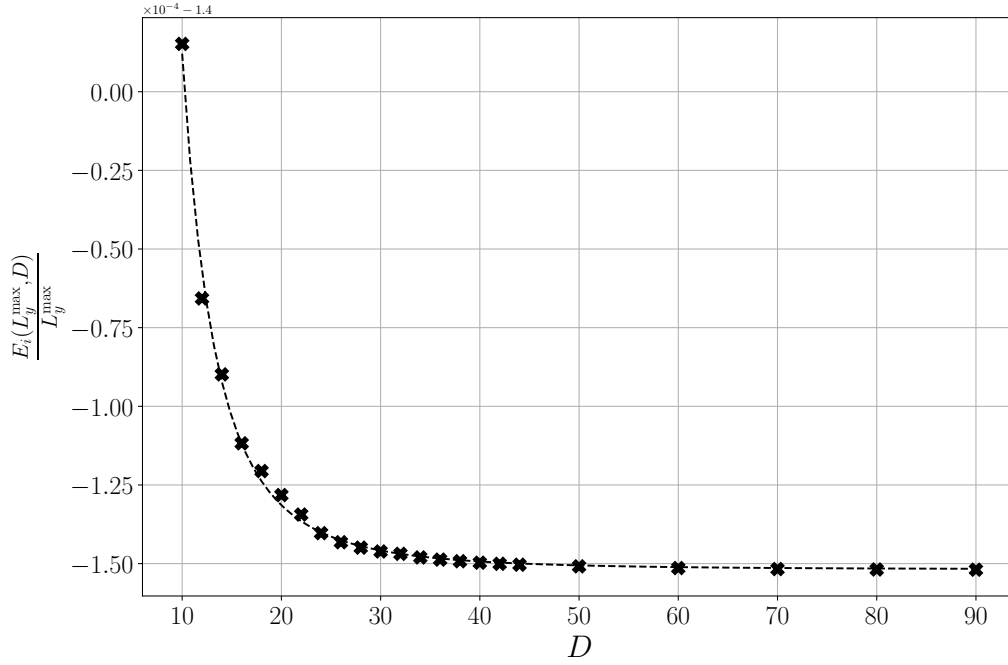


Figure 8. $\frac{E_i(T_c, L_y^{\max}, D)}{L_y^{\max}}$ as a function of D for $i=0$ (shifted by -1.4). Dashed line represents fitted result based on Eq. 13. Results for $i = 1, 2$ look identical at this scale and are not plotted. Here L_y^{\max} indicates the system size at which $E_i(L_y, D)/L_y$ becomes converged.

4. Conclusions and Discussions

In summary, we use recently proposed tensor network based finite-size scaling analysis to determine the critical temperature and critical exponents of the two-dimensional 3-state clock model. Due to the enhanced complexity more complicated crossover behavior is observed. However, by using the renormalization group concept and considering the relevant perturbation induced by the finite bond-dimension, we propose a strategy to identify the perihelion of the renormalization trajectory and use that system size to extract the best estimation of critical properties for a fixed set of parameters. Our results show that critical temperature can be estimated to extremely high accuracy. The relative error can be reduced to the order of 10^{-7} with $D = 70$ and $n = 3$. Consequently, the finite-size scaling analysis for other exponents can be carried out at the exact or best-estimated T_c . We find that with $D = 90$ and $n = 3$ the relative error for the critical exponents ν , β , and α can be reduced at least to the order of 10^{-3} . Moreover, in all cases our results indicate that the errors can be systematically reduced by increasing the bond dimension D and the stacking number n . It should be noted that results from \mathbb{Z}_3 symmetry HOTRG are reported here. We observe that in general HOTRG without enforcing the symmetry is less stable at large L and D , especially for quantities related to the order parameter. When the calculations are stable, however, the results

are consistent with the results reported here. In summary the benchmark on the 3-state clock model presented in this work, and the benchmark on the Ising model reported in Ref.[25] firmly establish that tensor network based finite-size scaling can be a powerful tool to study the phase transition and extract critical properties of 2D classical systems. It would be interesting to investigate various models using the methods presented in this work. For future directions, it is important and interesting to investigate how to generalize the method to study Berezinskii–Kosterlitz–Thouless transition, weakly first order transitions, and models in higher dimensions.

Acknowledgments

We acknowledge the support by National Science and Technology Council (NSTC) of Taiwan through Grants No. 110-2112-M-007-037-MY3 and No. 112-2119-M-007-008.

References

- [1] Kouichi Okunishi, Tomotoshi Nishino, and Hiroshi Ueda. Developments in the Tensor Network — from Statistical Mechanics to Quantum Entanglement. *J. Phys. Soc. Jpn.*, 91(6):062001, 2022.
- [2] Hiroshi Ueda, Kouichi Okunishi, Roman Krčmár, Andrej Gendiar, Seiji Yunoki, and Tomotoshi Nishino. Critical behavior of the two-dimensional icosahedron model. *Phys. Rev. E*, 96(6):062112, 2017.
- [3] Satoshi Morita and Naoki Kawashima. Calculation of higher-order moments by higher-order tensor renormalization group. *Comput. Phys. Commun.*, 236:65–71, 2019.
- [4] Hiroshi Ueda, Kouichi Okunishi, Seiji Yunoki, and Tomotoshi Nishino. Corner transfer matrix renormalization group analysis of the two-dimensional dodecahedron model. *Phys. Rev. E*, 102(3):032130, 2020.
- [5] Hiroshi Ueda, Kouichi Okunishi, Kenji Harada, Roman Krčmár, Andrej Gendiar, Seiji Yunoki, and Tomotoshi Nishino. Finite-m scaling analysis of Berezinskii-Kosterlitz-Thouless phase transitions and entanglement spectrum for the six-state clock model. *Phys. Rev. E*, 101(6):062111, 06 2020.
- [6] Atsushi Ueda and Masaki Oshikawa. Resolving the Berezinskii-Kosterlitz-Thouless transition in the two-dimensional XY model with tensor-network-based level spectroscopy. *Phys. Rev. B*, 104(16):165132, 2021.
- [7] G. Evenbly and G. Vidal. Tensor Network Renormalization. *Phys. Rev. Lett.*, 115(18):180405, 10 2015.
- [8] Guanrong Li, Kwok Ho Pai, and Zheng-Cheng Gu. Tensor-network renormalization approach to the q-state clock model. *Phys. Rev. Research*, 4(2):023159, 2022.
- [9] Wenhan Guo and Tzu-Chieh Wei. Tensor Network Methods for Extracting CFT Data from Fixed-Point Tensors and Defect Coarse Graining. *arXiv*, 2023.
- [10] Hiroshi Ueda, Kouichi Okunishi, and Tomotoshi Nishino. Doubling of entanglement spectrum in tensor renormalization group. *Phys. Rev. B*, 89(7):075116, 2014.
- [11] Zheng-Cheng Gu and Xiao-Gang Wen. Tensor-entanglement-filtering renormalization approach and symmetry-protected topological order. *Phys. Rev. B*, 80(15):155131, 2009.
- [12] Atsushi Ueda and Masahito Yamazaki. Fixed-point tensor is a four-point function. *arXiv*, 2023.
- [13] Gong Cheng, Lin Chen, Zheng-Cheng Gu, and Ling-Yan Hung. Exact fixed-point tensor network construction for rational conformal field theory. *arXiv*, 2023.
- [14] Michael Levin and Cody P Nave. Tensor Renormalization Group Approach to Two-Dimensional Classical Lattice Models. *Phys. Rev. Lett.*, 99(12):120601, 09 2007.

- [15] H. H. Zhao, Z. Y. Xie, Q. N. Chen, Z. C. Wei, J. W. Cai, and T. Xiang. Renormalization of tensor-network states. *Phys. Rev. B*, 81(17):174411, 2010.
- [16] Zhi-Yuan Xie, J Chen, Ming-Pu Qin, J W Zhu, L P Yang, and Tao Xiang. Coarse-graining renormalization by higher-order singular value decomposition. *Phys. Rev. B*, 86(4):045139, 07 2012.
- [17] Tomotoshi Nishino and Kouichi Okunishi. Corner Transfer Matrix Algorithm for Classical Renormalization Group. *J. Phys. Soc. Jpn.*, 66(10):3040 – 3047, 10 1997.
- [18] Román Orús and Guifré Vidal. Simulation of two-dimensional quantum systems on an infinite lattice revisited: Corner transfer matrix for tensor contraction. *Phys. Rev. B*, 80(9):094403, 2009.
- [19] Shuo Yang, Zheng-Cheng Gu, and Xiao-Gang Wen. Loop Optimization for Tensor Network Renormalization. *Phys. Rev. Lett.*, 118(11):110504, 03 2017.
- [20] B. Pirvu, G. Vidal, F. Verstraete, and L. Tagliacozzo. Matrix product states for critical spin chains: Finite-size versus finite-entanglement scaling. *Phys. Rev. B*, 86(7):075117, 2012.
- [21] Atsushi Ueda and Masaki Oshikawa. Finite-size and finite bond dimension effects of tensor network renormalization. *Phys. Rev. B*, 108(2):024413, 2023.
- [22] L. Tagliacozzo, Thiago. R. de Oliveira, S. Iblisdir, and J. I. Latorre. Scaling of entanglement support for matrix product states. *Phys. Rev. B*, 78(2):024410, 2008.
- [23] Seongpyo Hong and Dong-Hee Kim. Logarithmic finite-size scaling correction to the leading Fisher zeros in the p-state clock model: A higher-order tensor renormalization group study. *Phys. Rev. E*, 101(1):012124, 01 2020.
- [24] Ching-Yu Huang, Yuan-Chun Lu, and Pochung Chen. Finite-size scaling analysis of two-dimensional deformed Affleck-Kennedy-Lieb-Tasaki states. *Phys. Rev. B*, 102(16):165108, 2020.
- [25] Ching-Yu Huang, Sing-Hong Chan, Ying-Jer Kao, and Pochung Chen. Tensor network based finite-size scaling for two-dimensional Ising model. *Phys. Rev. B*, 107(20):205123, 2023.
- [26] Seongpyo Hong and Dong-Hee Kim. Tensor Network Calculation of the Logarithmic Correction Exponent in the XY Model. *J. Phys. Soc. Jpn.*, 91(8):084003, 2022.
- [27] Jorge V. José, Leo P. Kadanoff, Scott Kirkpatrick, and David R. Nelson. Renormalization, vortices, and symmetry-breaking perturbations in the two-dimensional planar model. *Phys. Rev. B*, 16(3):1217–1241, 1977.
- [28] F. Y. Wu. The Potts model. *Rev. Mod. Phys.*, 54(1):235–268, 1982.
- [29] R. B. Potts. Some generalized order-disorder transformations. *Math. Proc. Cambridge Philos. Soc.*, 48(1):106–109, 1952.
- [30] Jing Chen, Hai-Jun Liao, Hai-Dong Xie, Xing-Jie Han, Rui-Zhen Huang, Song Cheng, Zhong-Chao Wei, Zhi-Yuan Xie, and Tao Xiang. Phase Transition of the q-State Clock Model: Duality and Tensor Renormalization. *Chin. Phys. Lett.*, 34(5):050503, 05 2017.
- [31] A. Faissal Brito, José Arnaldo Redinz, and J. A. Plascak. Dynamics of rough surfaces generated by two-dimensional lattice spin models. *Phys. Rev. E*, 75(4):046106, 2007.
- [32] A. Faissal Brito, José Arnaldo Redinz, and J. A. Plascak. Two-dimensional XY and clock models studied via the dynamics generated by rough surfaces. *Phys. Rev. E*, 81(3):031130, 2010.
- [33] Seung Ki Baek and Petter Minnhagen. Non-Kosterlitz-Thouless transitions for the q-state clock models. *Phys. Rev. E*, 82(3):031102, 2010.
- [34] Yusuke Tomita and Yutaka Okabe. Finite-size scaling of correlation ratio and generalized scheme for the probability-changing cluster algorithm. *Phys. Rev. B*, 66(18):180401(R), 2002.
- [35] Jan Tobochnik. Properties of the q-state clock model for q=4, 5, and 6. *Phys. Rev. B*, 26(11):6201–6207, 1982.
- [36] Zi-Qian Li, Li-Ping Yang, Z. Y. Xie, Hong-Hao Tu, Hai-Jun Liao, and T. Xiang. Critical properties of the two-dimensional q-state clock model. *Phys. Rev. E*, 101(6):060105, 2020.
- [37] Q. N. Chen, M. P. Qin, J. Chen, Z. C. Wei, H. H. Zhao, B. Normand, and T. Xiang. Partial Order and Finite-Temperature Phase Transitions in Potts Models on Irregular Lattices. *Phys. Rev. Lett.*, 107(16):165701, 2011.

- [38] Tom Kennedy and Slava Rychkov. Tensor RG Approach to High-Temperature Fixed Point. *Journal of Statistical Physics*, 187(3):33, 2022.
- [39] C. N. Yang. The Spontaneous Magnetization of a Two-Dimensional Ising Model. *Physical Review*, 85(5):808–816, 1952.
- [40] Vid Stojevic, Jutho Haegeman, I. P. McCulloch, Luca Tagliacozzo, and Frank Verstraete. Conformal data from finite entanglement scaling. *Physical Review B*, 91(3):035120, 01 2015.